Estuarine acidification and minimum buffer zone—A conceptual study

Xinping Hu[1] and Wei-Jun Cai[2]

Received 3 September 2013; revised 16 September 2013; accepted 26 September 2013; published 7 October 2013.

[1] This study uses a simulation method to explore how estuarine pH is affected by mixing between river water, anthropogenic CO_2 enriched seawater, and by respiration. Three rivers with different levels of weathering products (Amazon, Mississippi, and St. Johns) are selected for this simulation. The results indicate that estuaries that receive low to moderate levels of weathering products (Amazon and St. Johns) exhibit a maximum pH decrease in the midsalinity region as a result of anthropogenic CO_2 intrusion. This maximum pH decrease coincides with a previously unrecognized mid-salinity minimum buffer zone (MBZ). In addition, water column oxygen consumption can further depress pH for all simulated estuaries. We suggest that recognition of the estuarine MBZs may be important for studying estuarine calcifying organisms and pH-sensitive biogeochemical processes. **Citation:** Hu, X., and W.-J. Cai (2013), Estuarine acidification and minimum buffer zone—A conceptual study, *Geophys. Res. Lett.*, *40*, 5176–5181, doi:10.1002/grl.51000.

1. Introduction

[2] In recent years, ocean acidification studies have expanded into coastal and estuarine waters [*Cai et al*., 2011; *Sunda and Cai*, 2012; *Wootton et al*., 2008]. These areas host many economically valuable animal species (e.g., shellfish) [*Dickinson et al*., 2012; *Miller et al*., 2009; *Tomanek et al*., 2011] and deteriorating vegetated habitats (e.g., seagrass meadows) [*Waycott et al*., 2009]. Sensitivity to acidification in these areas is thus more concerning than in the open ocean because acidification potentially has a more immediate effect on the health of estuarine and nearshore ecosystems as well as regional economies. For example, losses in shellfish harvesting from both natural fishing grounds and aquaculture have been reported in the literature recently [*Feely et al*., 2008, 2010], and high CO_2 exposure has been demonstrated to affect shellfish species at different life stages [*Barton et al*., 2012; *Dickinson et al*., 2012; *Gazeau et al*., 2007; *Hettinger et al*., 2012; *Kurihara et al*., 2007; *Parker et al*., 2010; *Waldbusser et al*., 2013]. In addition to ocean acidification caused by rising atmospheric CO_2, respiration of organic matter also produces CO_2; together with high levels of dissolved inorganic carbon (DIC) from upwelled seawater, these factors can seriously acidify coastal and estuarine waters [*Feely et al*., 2010]. This type of acidification is especially worrisome in stratified estuarine bottom waters [*Cai et al*., 2011; *Mucci et al*., 2011] where air-sea exchange is restricted. In addition to CO_2-induced acidification, rivers that flow through drainage basins that have acidic sulfate soils could also bring sulfuric acid into estuaries and cause serious acidification in estuarine waters [e.g., *Sammut et al*., 1995].

[3] The susceptibility of estuarine waters to acidification has been attributed to the lower buffer capacity from their alkalinity, which is lower than that in the ocean water [*Miller et al*., 2009]. However, not all estuaries are equal. It is unknown how estuarine buffer capacity along an estuarine salinity gradient changes, how it varies among rivers that carry different levels of bicarbonate as a result of drainage basin weathering (and to some extent due to land use changes such as in the Mississippi drainage basin) [e.g., *Raymond et al*., 2008], and how estuaries' buffer capacities would change in response to ocean acidification. Furthermore, in situ respiration will further affect the estuarine carbonate systems and also needs to be evaluated.

[4] In this work, we examine the pH and buffer behavior of estuarine waters using a series of simulations. Different freshwater end-members with different levels of weathering products are included in this discussion, together with the effects of respiration. Based on the result, we propose a new designation—the estuarine minimum buffer zone (MBZ).

2. Method

[5] We simulated three river-ocean mixing scenarios that involve three representative rivers (Table 1): a tropical river (Amazon) with a drainage basin that has low concentrations of weathering products, a mid-latitude river (Mississippi) with a drainage basin that has high concentrations of weathering products, and a mid-latitude river with a drainage basin that has moderate concentrations of weathering products (St. Johns, ME, USA). The rationale for using these rivers is because of their distinct carbonate chemistries, ranging from the relatively well-buffered Mississippi River to the low to moderately buffered Amazon and St. Johns Rivers, and because these rivers are distributed across different climate zones.

[6] For simplicity of discussion and easier comparison, we use a single Atlantic Ocean surface water at salinity 36 and alkalinity 2364.7 $\mu eq\,kg^{-1}$ [see *Millero et al*., 1998, Table 3] as the ocean end-member. Because we will be discussing the influence of increasing atmospheric CO_2 on the estuarine water carbonate chemistry, we use two different atmospheric CO_2 levels (280 ppmv during the preindustrial period and 800 ppmv in year 2100 according the "business-as-usual" scenario) [*Intergovernmental Panel on Climate Change (IPCC)*, 2001] to illustrate the changes in estuarine pH due to anthropogenic CO_2 intrusion. Because both river water and ocean water have been experiencing an increase in

Additional supporting information may be found in the online version of this article.

[1]Department of Physical and Environmental Sciences, Texas A&M University-Corpus Christi, Corpus Christi, Texas, USA.
[2]College of Earth, Ocean, Environment, University of Delaware, Newark, Delaware, USA.

Corresponding author: X. Hu, Department of Physical and Environmental Sciences, Texas A&M University-Corpus Christi, Corpus Christi, TX 78412, USA. (xinping.hu@tamucc.edu)

©2013. American Geophysical Union. All Rights Reserved.
0094-8276/13/10.1002/grl.51000

Table 1. Carbonate Chemistry in Amazon, Mississippi, and St. Johns Rivers

Name	C-Alk[a] (μmol kg^{-1})	DIC (μmol kg^{-1})	Temperature Range (°C)[b]	Reference
Amazon	265[a]	360	27–29	*Cooley* [2006]; *Devol et al.* [1995]
Mississippi	2237	2267	24–26	*Guo et al.* [2012]
St. Johns	592[a]	801	15–17	*Hunt et al.* [2011]

[a]C-Alk represents carbonate alkalinity in rivers, and the value is calculated by subtracting organic alkalinity in both the Amazon (35 μmol kg^{-1}) [*Devol et al.*, 1995] and St. Johns Rivers (293 μmol kg^{-1}) [*Hunt et al.*, 2011] from total alkalinity (300 μmol kg^{-1} and 885 μmol kg^{-1}, respectively). For the Mississippi River, we assume that the organic alkalinity contribution is negligible as pCO_2 calculated using TA and DIC agrees well with measured values [*Guo et al.*, 2012].
[b]Temperature is assumed to increase 2°C from the preindustrial time to year 2100.

temperature [*IPCC*, 2001; *Kaushal et al.*, 2010], in this work, we assume that all these estuaries will undergo a 2°C temperature increase from the preindustrial period to 2100. The average temperatures in Table 1 represent present conditions.

[7] To examine the respiration effect, for simplicity of discussion, we assume the remineralization of organic matter follows Redfield stoichiometry:

$$(CH_2O)_{106}(NH_3)_{16}(H_3PO_4)+138O_2 \rightarrow 106CO_2 + 16HNO_3 + H_3PO_4 + 122H_2O. \quad (1)$$

[8] Then we assume that respiration consumes 50% of the dissolved O_2 with waters being initially O_2 saturated. Thus, further pH changes caused by this hypothetical metabolic CO_2 addition, along with the minor alkalinity reduction due to acid production (equation (1)), can be calculated.

[9] To examine the magnitude of pH change between the preindustrial time and 2100, we define $\Delta pH = pH_{2100} - pH_{preindustrial}$. First, we contend that seawater is "saturated" with respect to the atmospheric CO_2 due to air-sea equilibrium in both the preindustrial period and year 2100, whereas river water has no anthropogenic CO_2 signal due to its generally much higher CO_2 partial pressure (pCO_2) compared to atmospheric values [e.g., *Butman and Raymond*, 2011]. Thus, the concentration of anthropogenic CO_2 (C_{ant}) in estuarine waters is proportional to the water salinity as a result of conservative river-ocean mixing:

$$C_{ant}(\text{estuary}) = C_{ant}(\text{sea})/S_{sea} \times S_{estuary} \quad (2)$$

Here $S_{estuary}$ and S_{sea} are salinities of the estuarine water and the seawater end-members, C_{ant} (estuary) and C_{ant} (sea) are the anthropogenic CO_2 levels of the estuary and the seawater end-members, respectively. C_{ant} (sea) can be calculated using seawater alkalinity by assuming the seawater is equilibrated with the two different air CO_2 levels at the chosen simulation temperatures (Table S1 in the supporting information).

[10] The MatLab® version of the program CO2SYS [*Lewis and Wallace*, 1998] was used to run the simulations. Carbonic acid dissociation constants are from *Millero* [2010], the bisulfate dissociation constant is from *Dickson and Riley* [1979], and the borate to salinity ratio is from *Uppström* [1974].

3. Results

[11] The pH (here we use total pH scale throughout this discussion) in both the Amazon and St. Johns estuaries starts from relatively low values (6.8–6.9) at the river end-members and increases toward the ocean end-members (Figures 1a and 1c). In comparison, pH in the Mississippi estuary shows a much smaller variation along the salinity gradient and the freshwater is slightly alkaline (pH >8) (Figure 1b).

[12] Intuitively, one may expect that ΔpH as a result of C_{ant} intrusion would follow the proportion of C_{ant} present in the estuarine water due to river-sea mixing (e.g., equation (2)), i.e., the magnitude of ΔpH approaches zero monotonically toward the river end-member as C_{ant} decreases linearly with

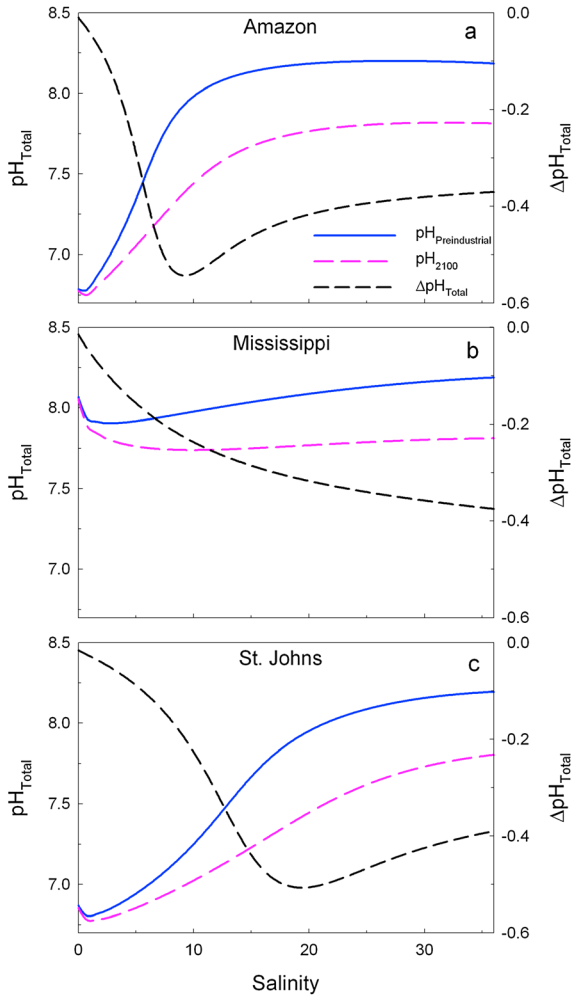

Figure 1. The pH in the preindustrial period (solid blue line) and 2100 (dashed pink line) in the (a) Amazon, (b) Mississippi, and (c) St. Johns estuaries, with pH decreases (ΔpH, dashed black line) as a result of C_{ant} addition from the preindustrial period to 2100. Temperature in 2100 is assumed to be 2°C warmer than in the preindustrial period.

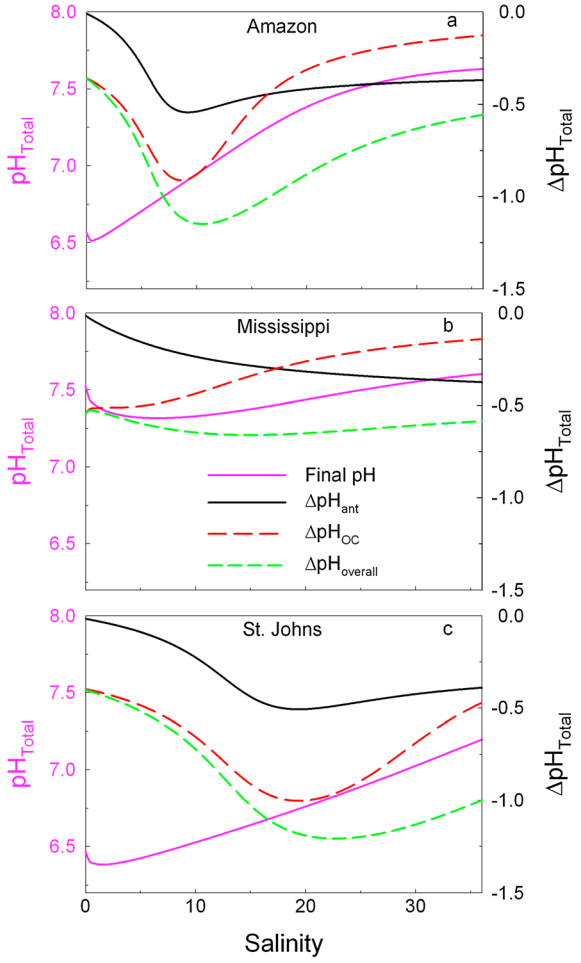

Figure 2. Changes in pH as a result of C_{ant} addition (ΔpH_{ant}, solid black line) or 50% oxygen consumption (ΔpH_{oc}, dashed red line) in the (a) Amazon, (b) Mississippi, and (c) St. Johns estuaries from the preindustrial conditions. The dashed green lines represent the overall pH change ($\Delta pH_{overall}$) due to the combined C_{ant} addition and oxygen consumption, and the solid pink lines represent the final pH at each estuary as a result of C_{ant} addition and 50% oxygen consumption. Temperature in 2100 is assumed to be 2°C warmer than in the preindustrial period.

salinity. However, for both the Amazon and St. Johns estuaries, first, there is a maximum pH decrease (i.e., most negative ΔpH) as salinity decreases, then ΔpH diminishes as salinity approaches zero (Figures 1a and 1c); whereas the expected ΔpH trend based on the amount of C_{ant} is only seen in the Mississippi estuary (Figure 1b). Furthermore, across the salinity gradients of the Amazon and St. Johns estuaries, under selected simulation temperature regimes (Table 1), the maximum pH decrease in the Amazon estuary occurs at salinity ~9, while for the St. Johns estuary, the same salinity is ~19 (Figure 1c).

[13] Finally, regardless of the river water chemistry, oxygen consumption in the water column can further decrease pH (ΔpH_{oc}, dashed red line in Figure 2) as was illustrated in earlier work [*Cai et al*., 2011; *Sunda and Cai*, 2012]. If we assume 50% oxygen consumption from the saturation values across the salinity gradient and that overlaying ΔpH_{oc} onto C_{ant} caused the pH decrease (ΔpH_{ant}, solid black line), the maximum pH decreases ($\Delta pH_{overall}$, dashed green line) in all three estuaries (i.e., −1.2, −0.7, and −1.2 pH units in Amazon, Mississippi, and St. Johns, respectively) are much greater than the ΔpH_{ant} alone (~0.5 pH units, Figure 2). A greater pH decrease caused by oxygen consumption than by C_{ant} intrusion across the salinity gradient in the St. Johns estuary can be attributed to higher oxygen solubility at lower temperature (Figure 2c). Consistent with C_{ant} induced pH decrease, the most negative $\Delta pH_{overall}$ also occurs at a higher salinity in the St. Johns estuary (Figure 2c) than in the Amazon estuary (Figure 2a).

4. Discussion

[14] The seemingly peculiar behavior of ΔpH along the salinity gradient can be explained by the relative changes in buffer behaviors in these three estuaries that have different carbonate chemistries. Typically, the Revelle factor [*Revelle and Suess*, 1957] is used when a quantitative examination of the responses of the carbonate system to CO_2 addition is needed. However, pH responses as a result of CO_2 addition cannot be determined explicitly using the Revelle factor. Therefore, we choose the β_{DIC} factor proposed by *Egleston et al*. [2010] as this factor provides a more direct measure of the pH response due to DIC addition:

$$\beta_{DIC} = \left(\frac{\partial \ln[H^+]}{\partial DIC}\right)^{-1}. \quad (3)$$

Here a decrease in β_{DIC} indicates a decrease in buffer capacity. The results (Figure 3) suggest that the buffer capacity of the Mississippi estuary increases monotonically with increasing salinity. However, for the Amazon and St. Johns estuaries, a minimum buffer zone (MBZ) appears in the midsalinity region that closely corresponds to the most negative ΔpH in each estuary due to C_{ant} intrusion (Figure 3). With increasing C_{ant} concentration in estuarine water, the MBZ is moving toward higher salinities (i.e., the dashed lines in Figure 3). Therefore, the maximum pH decrease in these two estuaries is a combination of the minimum buffer

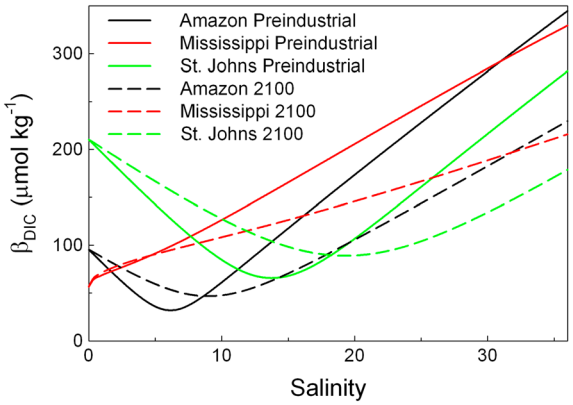

Figure 3. Buffer factor β_{DIC} as calculated using mixing between the river end-member and seawater end-members. The solid lines show the results for mixing with preindustrial seawater, and the dashed lines show the results for mixing with seawater saturated with atmospheric CO_2 at the 2100 level. Temperature in 2100 is assumed to be 2°C warmer than in the preindustrial period.

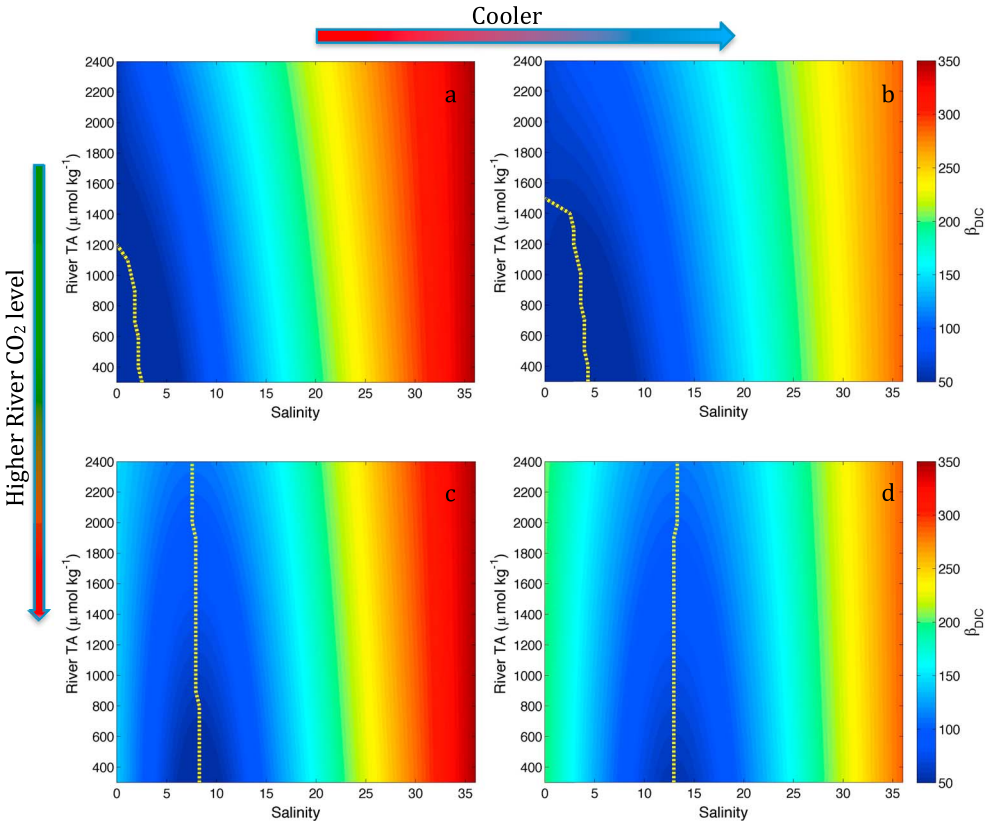

Figure 4. Estuarine water β_{DIC} as a function of salinity and alkalinity. Two temperatures (28°C and 16°C) and two river CO_2 levels (1200 and 4600 µatm) are chosen for this simulation: (a) 1200 µatm and 28°C, (b) 1200 µatm and 16°C, (c) 4600 µatm and 28°C, and (d) 1200 µatm and 16°C. The dotted yellow lines indicate the locations of the minimum β_{DIC}. For Figures 4a and 4b, minimum β_{DIC} appears at the freshwater end-member when river alkalinity is greater than 1200 and 1500 µmol kg^{-1}, respectively.

capacity and the amount of C_{ant} present in estuarine waters (equation (2)). An alternative explanation for the minimum buffer zone is that it occurs at a salinity where the estuarine pH approximately equal $(pK_1 + pK_2)/2$, where pK_1 and pK_2 are dissociation constants of carbonic acid (Figure S1).

[15] It is worth noting that once the salinity is below the MBZ salinity, β_{DIC} increases with decreasing salinity in both the Amazon and St. Johns estuaries (Figure 3). This increase simply reflects that there are very low levels of CO_3^{2-} (compared to those in the Mississippi estuary, Figure S2) to neutralize additional CO_2; thus, further addition of DIC mostly leads to an increase of the dissolved aqueous CO_2, or $CO_{2(aq)}$ [*Egleston et al.*, 2010]. In other words, the buffering of the DIC addition is thus based on dilution of DIC into the existing $CO_{2(aq)}$ pool, and subsequently, the pH (or $[H^+]$) change becomes less sensitive to further DIC additions when compared with that at the MBZ.

[16] In addition to the seawater C_{ant}-caused MBZ shift (Figure 3), both river carbonate chemistry and temperature play an important role in determining the location of the MBZ. If we consider a range of river alkalinity of 300–2400 µmol kg^{-1}, at two temperatures (28°C and 16°C) and two river pCO_2 levels (1200 µatm and 4600 µatm), which correspond to the upper and lower limits of the river parameters considered in this simulation, we can calculate the distribution of $\boldsymbol{\beta}_{DIC}$ as a function of river alkalinity and salinity by assuming that the river waters mix with preindustrial seawater. The results (Figure 4) suggest that the MBZ occurs in higher salinity waters when the river pCO_2 is high (i.e., higher DIC) or temperature is low. Therefore, rivers enriched in DIC as a result of respiration (thus having a higher DIC/TA ratio) at higher latitude (i.e., colder climate) should have their MBZs occurring closer to the ocean than those at lower latitude with low DIC/TA ratios (Figure 4d versus 4a). On the other hand, for a river with high alkalinity (> ~1600 µmol kg^{-1}) but moderate river pCO_2 such as the Mississippi, the MBZ does not exist (Figures 4a and 4b) under our examined temperature range. However, if the river pCO_2 was high enough (due to remineralization of riverine organic carbon), even estuaries that receive high alkalinity freshwater input would start to have an MBZ (Figure 4c).

[17] This study is the first that examines estuarine acidification caused by the increase in anthropogenic CO_2 in the ocean, in situ respiration, and river carbonate chemistry fluctuations. Earlier, *Sunda and Cai* [2012] simulated acidification caused by eutrophication-induced excess respiration in stratified estuarine bottom waters along a salinity gradient. However, they used a 1 mmol kg^{-1} alkalinity model river end-member without taking variability in river carbonate chemistry into account. Furthermore, they treated the C_{ant} signal along the salinity gradient by assuming equilibration with the atmosphere under different air CO_2 levels but not with the amount of C_{ant} that would be introduced through mixing with the ocean water. On the other hand, *Salisbury et al.* [2008] explored carbonate saturation states in various world river estuaries, although they did not consider the acidification effect in the estuaries caused by increases in seawater C_{ant}.

[18] Based on the simulation results, the Mississippi estuary shows the most resistance to acidification by having the least overall pH reduction under both C_{ant} influence alone and combined with DIC input from anthropogenic and respiration sources. Also, pH in this estuary remains the highest throughout most of the salinity gradient (Figure 2b). Therefore, given the high pH in warm estuaries such as the Mississippi estuary, these environments likely would remain habitable for calcifying organisms for the longest extent under current and predicted ocean acidification conditions. Moreover, compared with the estuaries on the east coast of the United States, the higher growth rate of bivalves in the Gulf of Mexico coastal estuaries [*Eastern Oyster Biological Review Team*, 2007], where river discharge of higher levels of weathering products occurs [*Benoit et al*., 1994], should at least partially contribute to a more favorable carbonate chemistry.

[19] The appearance of the MBZ in the midsalinity regions of estuaries with low to moderate levels of weathering products such as bicarbonate (e.g., Amazon and St. Johns) suggests that waters in the MBZs are extra sensitive to acidification stress, regardless of the acid source (CO_2, acidic soil, and nitrogen deposition). Recently, a long-term (1985–2010) pH decline was reported in the polyhaline ($S > 18$) waters of the Chesapeake Bay [*Waldbusser et al*., 2011] with a pH decrease of -0.006 to -0.012 year^{-1}, which is far greater than the rate in the open ocean during the same time frame (-0.0017 year^{-1}) [*Byrne et al*., 2010; *González-Dávila et al*., 2007]. While the detailed carbonate system chemistry during this long-term observation is unknown, we propose that the MBZ may have played an important role in pH regulations in this estuary, and further study would be needed to examine this hypothesis. Furthermore, we hypothesize that reduced pH in the midsalinity waters probably has already taken a toll on both the settlement efficiency of juvenile calcifiers (by extending the duration of pelagic phase) and the well-being of benthic adult individuals and populations [*Waldbusser et al*., 2011, and references therein].

[20] Other than the effect of pH on calcification, many biogeochemical reactions are pH-sensitive. For example, ammonia oxidation strongly depends on the environmental pH although exactly how pH mediates such reactions is not without controversy [*Fulweiler et al*., 2011; *Kitidis et al*., 2011]. Given the fact that estuaries are important locations for removing fixed nitrogen [*Seitzinger et al*., 2006], further studies on changes in pH due to acidification within estuaries, and subsequently, how such pH change would affect the nitrogen cycle is probably an important research topic in these dynamic systems.

[21] Finally, this work discusses highly simplified scenarios that only consider the conservative mixing of river water and ocean water, and water pH is controlled mostly by the carbonate system (and borate to a much smaller extent, in the calculations of β_{DIC} and pH using CO2SYS). In nature, however, estuarine biogeochemical reactions that involve proton production and consumption are rather complex (for example, the presence of organic acid and other acid-base species) and are often accompanied by nonconservative mixing behaviors [e.g., *Cifuentes et al*., 1990]; therefore, MBZs may not appear exactly at the salinities predicted using the conservative mixing model. Nevertheless, the MBZ should remain a fundamental estuarine property governed by acid-base chemistry. Under the context of ocean acidification, it would be of great interest to differentiate the long-term estuarine pH trends due to oceanic CO_2 uptake from the short-term variations due to biogeochemical reactions, the latter probably being larger in magnitude, in many disparate estuarine systems.

[22] **Acknowledgments.** This study was supported by the startup fund to XH provided by the College of Science and Engineering at Texas A&M University-Corpus Christi. We thank the Associate Editor and two anonymous reviewers for their critical comments that helped to improve the quality of this work. We also thank S. Cooley for her thorough editorial assistance.

[23] The Editor thanks an anonymous reviewer for assisting in the evaluation of this paper.

References

Barton, A., B. Hales, G. G. Waldbusser, C. Langdon, and R. A. Feely (2012), The Pacific oyster, *Crassostrea gigas*, shows negative correlation to naturally elevated carbon dioxide levels: Implications for near-term ocean acidification effects, *Limnol. Oceanogr.*, *57*, 698–710.

Benoit, G., S. D. Oktay-Marshall, A. Cantu II, E. M. Hood, C. H. Coleman, M. O. Corapcioglu, and P. H. Santschi (1994), Partitioning of Cu, Pb, Ag, Zn, Fe, Al, and Mn between filter-retained particles, colloids, and solution in six Texas estuaries, *Mar. Chem.*, *45*, 307–336.

Butman, D., and P. A. Raymond (2011), Significant efflux of carbon dioxide from streams and rivers in the United States, *Nat. Geosci.*, *4*, 839–842.

Byrne, R. H., S. Mecking, R. A. Feely, and X. Liu (2010), Direct observations of basin-wide acidification of the North Pacific Ocean, *Geophys. Res. Lett.*, *37*, L02601, doi:10.1029/2009GL040999.

Cai, W.-J., et al. (2011), Acidification of subsurface coastal waters enhanced by eutrophication, *Nat. Geosci.*, *4*, 766–770.

Cifuentes, L. A., L. E. Schemel, and J. H. Sharp (1990), Qualitative and numerical analyses of the effects of river inflow variations on mixing diagrams in estuaries, *Estuar. Coast. Shelf Sci.*, *30*, 411–427.

Cooley, S. R. (2006), Dissolved inorganic carbon cycling in the offshore Amazon River plume and the western tropical North Atlantic ocean, PhD thesis, 298 pp., University of Georgia, Athens.

Devol, A. H., B. R. Forsberg, J. E. Richey, and T. P. Pimentel (1995), Seasonal variation in chemical distributions in the Amazon (Solimões) River: A multiyear time series, *Global Biogeochem. Cycles*, *9*, 307–328.

Dickinson, G. H., A. V. Ivanina, O. B. Matoo, H. O. Pörtner, G. Lannig, C. Bock, E. Beniash, and I. M. Sokolova (2012), Interactive effects of salinity and elevated CO_2 levels on juvenile eastern oysters, *Crassostrea virginica*, *J. Exp. Biol.*, *215*, 29–43.

Dickson, A. G., and J. P. Riley (1979), The estimation of acid dissociation constants in seawater media from potentionmetric titrations with strong base. I. The ionic product of water — Kw, *Mar. Chem.*, *7*, 89–99.

Eastern Oyster Biological Review Team (2007), Status review of the eastern oyster (*Crassostrea virginica*). Report to the National Marine Fisheries Service, Northeast Regional Office. February 16, 2007, 105 pp., NOAA Tech. Memo. NMFS F/SPO-88.

Egleston, E. S., C. L. Sabine, and F. M. M. Morel (2010), Revelle revisited: Buffer factors that quantify the response of ocean chemistry to changes in DIC and alkalinity, *Global Biogeochem. Cycles*, *24*, GB1002, doi:10.1029/2008GB003407.

Feely, R. A., C. L. Sabine, J. Martin Hernandez-Ayon, D. Ianson, and B. Hales (2008), Evidence for upwelling of corrosive "acidified" water onto the continental shelf, *Science*, *320*, 1490–1492.

Feely, R. A., S. R. Alin, J. Newton, C. L. Sabine, M. Warner, A. Devol, C. Krembs, and C. Maloy (2010), The combined effects of ocean acidification, mixing, and respiration on pH and carbonate saturation in an urbanized estuary, *Estuar. Coast. Shelf Sci.*, *88*, 442–449.

Fulweiler, R., H. E. Emery, E. M. Heiss, and V. M. Berounsky (2011), Assessing the role of pH in determining water column nitrification rates in a coastal system, *Estuarine Coastal*, *34*, 1095–1102.

Gazeau, F., C. Quiblier, J. M. Jansen, J.-P. Gattuso, J. J. Middelburg, and C. H. R. Heip (2007), Impact of elevated CO_2 on shellfish calcification, *Geophys. Res. Lett.*, *34*, L07603, doi:10.1029/2006GL028554.

González-Dávila, M., J. Magdalena Santana-Casiano, and E. F. González-Dávila (2007), Interannual variability of the upper ocean carbon cycle in the northeast Atlantic Ocean, *Geophys. Res. Lett.*, *34*, L07608, doi:10.1029/2006GL028145.

Guo, X., et al. (2012), CO_2 dynamics and community metabolism in the Mississippi River plume, *Limnol. Oceanogr.*, *57*, 1–17.

Hettinger, A., E. Sanford, T. M. Hill, A. D. Russell, K. N. S. Sato, J. Hoey, M. Forsch, H. N. Page, and B. Gaylord (2012), Persistent carry-over effects of planktonic exposure to ocean acidification in the Olympia oyster, *Ecology*, *93*, 2758–2768.

Hunt, C. W., J. E. Salisbury, and D. Vandemark (2011), Contribution of non-carbonate anions to river alkalinity and overestimation of pCO_2

in New England and New Brunswick rivers, *Biogeosciences*, *8*, 3069–3076.

Intergovernmental Panel on Climate Change (IPCC) (2001), Climate change 2001: The scientific basis.

Kaushal, S. S., G. E. Likens, N. A. Jaworski, M. L. Pace, A. M. Sides, D. Seekell, K. T. Belt, D. H. Secor, and R. L. Wingate (2010), Rising stream and river temperatures in the United States, *Front. Ecol. Environ.*, *8*, 461–466.

Kitidis, V., B. Laverock, L. C. McNeill, A. Beesley, D. Cummings, K. Tait, M. A. Osborn, and S. Widdicombe (2011), Impact of ocean acidification on benthic and water column ammonia oxidation, *Geophys. Res. Lett.*, *38*, L21603, doi:10.1029/2011GL049095.

Kurihara, H., S. Kato, and A. Ishimatsu (2007), Effects of increased seawater pCO_2 on early development of the oyster *Crassostrea gigas*, *Aquat. Biol.*, *1*, 91–98.

Lewis, E., and D. Wallace (1998), Program developed for CO_2 system calculations. ORNL/CDIAC-105., edited, Carbon Dioxide Information Analysis Center, Oak Ridge National Laboratory, U.S. Department of Energy, Oak Ridge, Tennessee.

Miller, A. W., et al. (2009), Shellfish face uncertain future in high CO_2 world: Influence of acidification on oyster larvae calcification and growth in estuaries, *PLoS ONE*, *4*, e5661.

Millero, F. J. (2010), Carbonate constants for estuarine waters, *Mar. Freshwater Res.*, *61*, 139–142.

Millero, F. J., K. Lee, and M. Roche (1998), Distribution of alkalinity in the surface waters of the major oceans, *Mar. Chem.*, *60*, 111–130.

Mucci, A., M. Starr, D. Gilbert, and B. Sundby (2011), Acidification of lower St. Lawrence estuary bottom waters, *Atmos. Ocean*, *49*, 206–218.

Parker, L., P. M. Ross, and W. A. O'Connor (2010), Comparing the effect of elevated pCO_2 and temperature on the fertilization and early development of two species of oysters, *Mar. Biol.*, *157*, 2435–2452.

Raymond, P. A., N.-H. Oh, R. E. Turner, and W. Broussard (2008), Anthropogenically enhanced fluxes of water and carbon from the Mississippi River, *Nature*, *451*, 449–452.

Revelle, R., and H. Suess (1957), Carbon dioxide exchange between atmosphere and ocean and the question of an increase of atmospheric CO_2 during the past decades, *Tellus*, *9*, 18–27.

Salisbury, J., M. Green, C. Hunt, and J. Campbell (2008), Coastal acidification by rivers: A threat to shellfish?, *Eos Trans. Am. Geophys. Union*, *89*, 513–514.

Sammut, J., M. D. Melville, R. B. Callinan, and G. C. Fraser (1995), Estuarine acidification: Impacts on aquatic biota of draining acid sulphate soils, *Aust. Geogr. Stud.*, *33*, 89–100.

Seitzinger, S., J. A. Harrison, J. K. Böhlke, A. F. Bouwman, R. Lowrance, B. Peterson, C. Tobias, and G. Van Drecht (2006), Denitrification across landscapes and waterscapes: A synthesis, *Ecol. Appl.*, *16*, 2064–2090.

Sunda, W. G., and W.-J. Cai (2012), Eutrophication induced CO_2-acidification of subsurface coastal waters: Interactive effects of temperature, salinity, and atmospheric pCO_2, *Environ. Sci. Technol.*, *46*, 10,651–10,659.

Tomanek, L., M. J. Zuzow, A. V. Ivanina, E. Beniash, and I. M. Sokolova (2011), Proteomic response to elevated pCO_2 level in eastern oysters, *Crassostrea virginica*: Evidence for oxidative stress, *J. Exp. Biol.*, *214*, 1836–1844.

Uppström, L. R. (1974), The boron/chlorinity ratio of deep-sea water from the Pacific Ocean, *Deep Sea Res. Oceanogr. Abstr.*, *21*, 161–162.

Waldbusser, G., E. P. Voigt, H. Bergschneider, M. A. Green, and R. I. E. Newell (2011), Biocalcification in the Eastern Oyster (*Crassostrea virginica*) in relation to long-term trends in Chesapeake Bay pH, *Estuar. Coast.*, *34*, 221–231.

Waldbusser, G. G., et al. (2013), A developmental and energetic basis linking larval oyster shell formation to acidification sensitivity, *Geophys. Res. Lett.*, *40*, 2171–2176, doi:10.1002/grl.50449.

Waycott, M., et al. (2009), Accelerating loss of seagrasses across the globe threatens coastal ecosystems, *Proc. Natl. Acad. Sci. U.S.A.*, *106*, 12,377–12,381.

Wootton, J. T., C. A. Pfister, and J. D. Forester (2008), Dynamic patterns and ecological impacts of declining ocean pH in a high-resolution multi-year dataset, *Proc. Natl. Acad. Sci. U.S.A.*, *105*, 18,848–18,853.